Li_2MnSiO_4 Lithium Battery Material: Atomic-Scale Study of Defects, Lithium Mobility, and Trivalent Dopants

ARTICLE *in* CHEMISTRY OF MATERIALS · NOVEMBER 2009

Impact Factor: 8.35 · DOI: 10.1021/cm902163k

CITATIONS
65

READS
59

2 AUTHORS:

Navaratnarajah Kuganathan
University of Oxford
48 PUBLICATIONS **466** CITATIONS

SEE PROFILE

M. Saiful Islam
University of Bath
175 PUBLICATIONS **7,445** CITATIONS

SEE PROFILE

5196 *Chem. Mater.* **2009,** *21,* 5196–5202
DOI:10.1021/cm902163k

CHEMISTRY OF MATERIALS
Article

Li_2MnSiO_4 Lithium Battery Material: Atomic-Scale Study of Defects, Lithium Mobility, and Trivalent Dopants

N. Kuganathan and M. S. Islam*

Department of Chemistry, University of Bath, Bath BA2 7AY, U.K.

Received July 16, 2009. Revised Manuscript Received September 15, 2009

A new family of silicate materials has attracted interest for potential use in rechargeable lithium batteries. The defect chemistry, doping behavior, and lithium diffusion paths in the Li_2MnSiO_4 cathode material are investigated by advanced modeling techniques. Our simulations show good reproduction of both monoclinic and orthorhombic structures of Li_2MnSiO_4. The most favorable intrinsic defect type is found to be the cation anti-site defect, in which Li and Mn ions exchange positions. The migration energies suggest differences in intrinsic Li mobility between the monoclinic and orthorhombic polymorphs, which would affect their rate capability as rechargeable electrodes. The results indicate curved Li diffusion paths and confirm the anisotropic nature of Li transport, which is probably general for the Li_2MSiO_4 (M = Mn, Fe, Co) family of compounds. Subvalent doping by Al on the Si site is energetically favorable and could be a synthesis strategy to increase the Li content.

1. Introduction

Energy storage through rechargeable lithium batteries has helped power the revolution in portable electronics. For the next generation of such batteries, there is intensive research activity in developing improved electrode materials particularly for use in hybrid electric vehicles to help promote low carbon transport.[1,2] Despite the investigations of a rich variety of electrode materials over the last two decades, no major increase in capacity has been achieved. Future breakthroughs in new materials are therefore crucial and depend on exploring novel classes of compounds and on a greater fundamental understanding of their properties.

Polyanion systems based on the olivine-phosphate $LiFePO_4$ have attracted considerable attention as viable alternatives to the conventional positive electrode material, $LiCoO_2$.[1−3] The structural stability and reasonably high redox potentials are provided by the orthophosphate anion (PO_4^{3-}) matrix, which has relatively strong P−O bonds. More recently, the orthosilicate family including Li_2FeSiO_4 and Li_2MnSiO_4 has been found to show good electrochemical performance as cathode materials.[4−16] The strong Si−O bonds should promote similar lattice stabilization effects found in the much-studied $LiFePO_4$ material. Moreover, silicon, iron, and manganese are relatively safe, abundant, and low-cost, which potentially makes these silicate materials more sustainable.

Thomas et al.,[4,5] Dominko et al.,[8−11] and Arroyo-de Dompablo et al.[13,14] have reported structural (XRD, XPS), electrochemical, and DFT studies on these silicates. A key feature of Li_2FeSiO_4 and Li_2MnSiO_4 is that, in principle, extraction of two lithiums is possible (for a two electron redox process); this should produce a higher capacity (e.g., above 300 mA h/g for Li_2MnSiO_4) than the olivine phosphates in which one lithium at most can be extracted.[8,9] In addition, it may be possible to remove more than one lithium more readily from Li_2MnSiO_4 than from Li_2FeSiO_4, since the higher manganese oxidation

*Corresponding author. Fax: +44-(0)1225-386231. E-mail: m.s.islam@bath.ac.uk.

(1) Armand, M.; Tarascon, J.-M. *Nature* **2008**, *451*, 652.
(2) (a) Whittingham, M. S. *Chem. Rev.* **2004**, *104*, 4271. (b) Arico, A. S.; Bruce, P.; Scrosati, B.; Tarascon, J. M.; Van Schalkwijk, W. *Nat. Mater.* **2005**, *4*, 366.
(3) Padhi, A. K.; Nanjundaswamy, K. S.; Goodenough, J. B. *J. Electrochem. Soc.* **1997**, *144*, 1188.
(4) Nyten, A.; Abouimrane, A.; Armand, M.; Gustafsson, T.; Thomas, J. O. *Electrochem. Commun.* **2005**, *7*, 156.
(5) (a) Nyten, A.; Kamali, S.; Haggstrom, L.; Gustafsson, T.; Thomas, J. O. *J. Mater. Chem.* **2006**, *16*, 2266. (b) Ensling, D.; Stjerndahl, M.; Nyten, A.; Gustafsson, T.; Thomas, J. O. *J. Mater. Chem.* **2009**, *19*, 82.
(6) Zaghib, K.; Salah, A. A.; Ravet, N.; Mauger, A.; Gendron, F.; Julien, C. M. *J. Power Sources* **2006**, *160*, 1381.
(7) Nishimura, S. I.; Hayase, S.; Kanno, R.; Yashima, M.; Nakayama, N.; Yamada, A. *J. Am. Chem. Soc.* **2008**, *130*, 13212.
(8) Dominko, R.; Bele, M.; Gaberscek, M.; Meden, A.; Remskar, M.; Jamnik, J. *Electrochem. Commun.* **2006**, *8*, 217.
(9) Kokalj, A.; Dominko, R.; Mali, G.; Meden, A.; Gaberscek, M.; Jamnik, J. *Chem. Mater.* **2007**, *19*, 3633.
(10) Dominko, R. *J. Power Sources* **2008**, *184*, 462.
(11) Dominko, R.; Arcon, I.; Kodre, A.; Hanzel, D.; Gaberscek, M. *J. Power Sources* **2009**, *189*, 51.
(12) Politaev, V. V.; Petrenko, A. A.; Nalbandyan, V. B.; Medvedev, B. S.; Shvetsova, E. S. *J. Solid State Chem.* **2007**, *180*, 1045.
(13) Arroyo-de Dompablo, M. E.; Armand, M.; Tarascon, J. M.; Amador, U. *Electrochem. Commun.* **2006**, *8*, 1292.
(14) Arroyo-DeDompablo, M. E.; Dominko, R.; Gallardo-Amores, J. M.; Dupont, L.; Mali, G.; Ehrenberg, H.; Jamnik, J.; Moran, E. *Chem. Mater.* **2008**, *20*, 5574.
(15) (a) Gong, Z. L.; Li, Y. X.; Yang, Y. *Electrochem. Solid State Lett.* **2006**, *9*, A542. (b) Zhang, S.; Deng, C.; Yang, S. Y. *Electrochem. Solid State Lett.* **2009**, *12*, A136. (c) Wu, S. Q.; Zhu, Z. Z.; Yang, Y.; Hou, Z. F. *Comput. Mater. Sci.* **2009**, *44*, 1243. (d) Ghosh, P.; Mahanty, S.; Basu, R. N. *J. Electrochem. Soc.* **2009**, *156*, A677.
(16) Lyness, C.; Delobel, B.; Armstrong, A. R.; Bruce, P. G. *Chem. Commun.* **2007**, 4890.

 Published on Web 10/09/2009

state Mn^{4+} is far more accessible than Fe^{4+}. However, current electrochemical studies have not achieved such high capacities.

As discussed by West and Glasser,[17] the orthosilicate compounds belong to a family of tetrahedral structures that exhibit a rich polymorphism. The parent compound for Li_2MSiO_4 is Li_3PO_4, which exists in two polymorphic forms (labeled β and γ) and is derived by replacing one Li by M and P by Si. In this context, it is worth mentioning the inorganic Li-ion conductors known as LISICONs, which have a related Li_3PO_4-type structure and are solid solutions derived from stoichiometric end members of, for example, Li_4GeO_4 and Li_2ZnGeO_4.[17]

There has been significant debate concerning the observed structures of Li_2MnSiO_4. From powder X-ray diffraction (XRD), Dominko et al.[8] proposed an orthorhombic structure (based on β-Li_3PO_4), which is isostructural with orthorhombic Li_2FeSiO_4 (space group $Pmn2_1$),[5] although they note at least one unidentified impurity phase in their data. The structural study by Nyten et al.[5] of orthorhombic Li_2FeSiO_4 shows a Li_2SiO_3 impurity phase and very short Li−Si distances. XRD studies of Li_2MnSiO_4 by Politaev et al.[12] find a structure of monoclinic symmetry (space group $P2_1/n$) based on γ-Li_3PO_4, similar to a recent report of monoclinic Li_2FeSiO_4 from XRD/TEM studies of Nishimura et al.[7]

Both monoclinic and orthorhombic Li_2MnSiO_4 polymorphs are based on a distorted hexagonal close-packed array of oxygen ions with all cations in corner-sharing tetrahedra but differ in the orientation of these tetrahedra, particularly for the MnO_4−SiO_4 chains (shown in Figure 1); the orthorhombic ($Pmn2_1$) structure has these MnO_4−SiO_4 tetrahedra all aligned in the same direction, whereas in the monoclinic ($P2_1/n$) structure the MnO_4−SiO_4 tetrahedra alternately point in opposite directions.

As well as these structural issues, it is well-known that the underlying defect and conduction properties of lithium battery cathode materials are complex on the atomic scale but are crucial to the greater understanding of the structure−composition−property relationships and the electrochemical behavior. The present study uses well-established atomistic modeling techniques to investigate key issues related to point defects, dopants, and lithium ion mobility in both the monoclinic and orthorhombic polymorphs of the Li_2MnSiO_4 material, with reference to experimental studies where possible. For instance, there has been discussion in the literature on Li/Mn mixing or anti-site disorder.[12] Also, a possible approach to increasing the capacity of the Li_2MnSiO_4 cathodes is to introduce additional lithium into the as-prepared materials. However, very little work has been performed in this area; hence, we have investigated the energetics of trivalent doping (e.g., Al) on the Si site compensated by extra lithium.

(17) (a) West, A. R.; Glasser, F. P. *J. Solid State Chem.* **1972**, *4*, 20. (b) West, A. R.; Glasser, F. P. *J. Mater. Sci.* **1970**, *5*, 557. (c) Bruce, P. G.; West, A. R. *Mater. Res. Bull.* **1980**, *15*, 379.

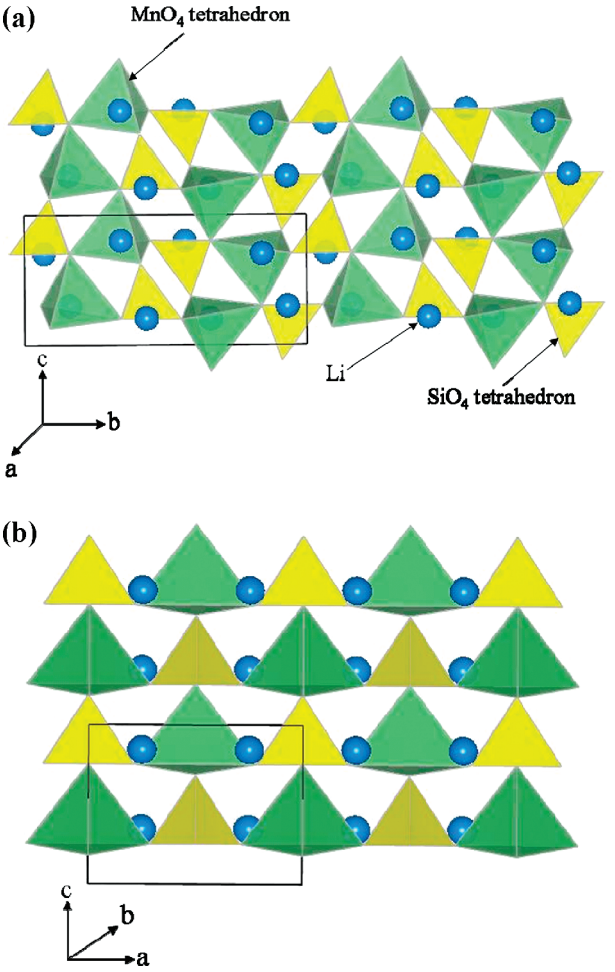

Figure 1. Crystal structures of Li_2MnSiO_4 polymorphs; (a) monoclinic (space group $P2_1/n$) and (b) orthorhombic (space group $Pmn2_1$).

The present work extends our previous simulation studies of the $LiMPO_4$ (M = Fe, Mn, Co, Ni) battery materials, where we examined the bulk defect chemistry and lithium transport,[18,19] and, more recently, surface structures and crystal morphologies of $LiFePO_4$.[20] In this study, we have examined both monoclinic and orthorhombic polymorphs of Li_2MnSiO_4 and carried out a detailed survey of the relative energetics of the formation of intrinsic defects, the incorporation of dopants, and the possible pathways for lithium ion conduction.

2. Simulation Methods

This investigation uses well-established simulation techniques based on the Born model of solids. As these techniques are described in detail elsewhere,[21] only a general outline will be given here. All systems were treated as crystalline solids, with interactions between ions consisting of a long-range Coulombic term and a short-range component representing electron−electron repulsion and

(18) Islam, M. S.; Driscoll, D. J.; Fisher, C. A. J.; Slater, P. R. *Chem. Mater.* **2005**, *17*, 5085.
(19) Fisher, C. A. J.; Hart Prieto, V. M.; Islam, M. S. *Chem. Mater.* **2008**, *20*, 5907.
(20) Fisher, C. A. J.; Islam, M. S. *J. Mater. Chem.* **2008**, *18*, 1209.
(21) Catlow, C. R. A. *Computer Modeling in Inorganic Crystallography*; Academic Press: San Diego, CA, 1997.

van der Waals interactions. The short-range interactions were modeled using the Buckingham potential,

$$\Phi_{ij}(r_{ij}) = A_{ij}\exp(-r_{ij}/\rho_{ij}) - C_{ij}/r_{ij}^{6} \quad (1)$$

where r is the interatomic separation and A, ρ, and C are ion−ion potential parameters. An additional three-body term was used for the SiO_4 units to take into account the angle-dependent nature of O−Si−O bonds, as used successfully for aluminosilicates (especially zeolites).[21,22] The three-body term takes the form of a harmonic angle-bending potential about the Si ion,

$$\Phi_{ijk} = \frac{1}{2}K_{ijk}(\theta - \theta_0)^2 \quad (2)$$

where K is the force constant and the angle θ_0 is the equilibrium bond angle for a SiO_4 tetrahedron. To provide a simple means of including effects of electronic polarization, we employed the shell model for Mn^{2+} and O^{2-} ions. This method allows the polarization effects of charged defects to be taken into account and has proven effective in simulating dielectric properties of a wide range of ceramic oxides. As argued previously,[21] employing a formal charge model does not necessarily mean that the electron distribution corresponds to a fully ionic system, as the validity of the potential model is assessed primarily by its ability to reproduce observed crystal properties. In practice it is found that such models work well, even for compounds where there is a degree of covalency, such as aluminosilcates[22] and olivine silicates.[23] A key benefit of the formal charge model is that there are no ambiguities about the charge state when considering isovalent and aliovalent dopant substitution.

The lattice relaxation about point defects, dopants, or migrating ions was calculated using an implementation of the Mott-Littleton scheme incorporated in the GULP code.[24] This method partitions a crystal lattice into two regions, with ions within the inner spherical region (on the order of >700 ions) immediately surrounding the defect relaxed explicitly. Relaxation of such a large number of ions is important for charged defects that introduce long-range electrostatic perturbations and is not easily treated by ab initio electronic structure methods. These atomistic simulation techniques have been used successfully on a wide range of inorganic solids, including energy-related materials for solid oxide fuel cells[25,26] and for lithium batteries.[18−20]

3. Results and Discussion

3.1. Structural Modeling. The starting point of the study was to reproduce the experimentally observed structures. As noted, there has been significant debate concerning the crystal structures of Li_2MnSiO_4. An orthorhombic structure has been proposed,[8] which is isostructural to orthorhombic Li_2FeSiO_4 (space group $Pmn2_1$),[5] although the final R-factor in the refinement was not reported. A monoclinic structure (space group $P2_1/n$) has also been proposed,[12] which is similar to that in a recent report of monoclinic Li_2FeSiO_4 from XRD/TEM studies.[7]

Both monoclinic and orthorhombic structures are based on a distorted hexagonal close-packed array of oxygen ions with all cations in corner-sharing tetrahedra but differ in the orientation of these tetrahedra (shown in Figure 1). Related computational work includes DFT calculations[9] on orthorhombic Li_2MnSiO_4 predicting that this phase is unstable on extraction of large amounts of lithium. Arroyo-de Dompablo et al.[14] reported DFT calculations on the thermodynamic stability of Li_2MnSiO_4 polymorphs predicting that the lowest energy is found for the β-Li_3PO_4-based derivatives.

In this study we have therefore examined both monoclinic and orthorhombic polymorphs of Li_2MnSiO_4. The interatomic potentials and shell charges were selected from previous published work relating to the atomistic modeling of olivine phosphate[18,19] and silicate materials.[21,22] The potentials and other parameters used in the present study are listed in Table 1.

The structures of Li_2MnSiO_4 were first optimized under constant pressure conditions, which allow both lattice parameters (cell volume) and ion positions to relax. The calculated and initial (experimental) structural parameters are listed in Table 2 and show good agreement for both structures. The calculated unit cell parameters and cation−oxygen bond lengths show a mean deviation from experiment of less than 0.07 Å. It is noted that the initial orthorhombic structure model for Li_2MnSiO_4 used the ion positions from the diffraction study of isostructural Li_2FeSiO_4 reported by Nyten et al.[5] and unit cell

Table 1. Interatomic Potential and Shell Model Parameters for Li_2MnSiO_4

(a) Two-Body

interaction	A (eV)	ρ (Å)	C (eV·Å^6)
Li^+-O^{2-}	632.1018	0.2906	0.00
$Mn^{2+}-O^{2-}$	2601.394	0.2780	0.00
$Si^{4+}-O^{2-}$	1283.91	0.32052	10.66
$O^{2-}-O^{2-}$	22764.30	0.1490	27.89

(b) Shell model

Species	Y (e)	K (eV·Å^{-2})
Li	1.000	99999
Mn	3.420	95.00
Si	4.000	99999
O	−2.860	74.92

(c) Three-body

bonds	k (eV·rad^{-2})[a]
O−Si−O	2.09724

[a] Experimental angles from refs 5 and 12.

(22) (a) Ojo, S. A.; Whitmore, L.; Slater, B.; Catlow, C. R. A. *Solid State Sci.* **2001**, *3*, 821. (b) Slater, B.; Titiloye, J. O.; Higgins, F. M.; Parker, S. C. *Curr. Opin. Solid State Mater. Sci.* **2001**, *5*, 417.
(23) Walker, A. M.; Wright, K.; Slater, B. *Phys. Chem. Miner.* **2003**, *30*, 536.
(24) Gale, J. D.; Rohl, A. L. *Mol. Simul.* **2003**, *29*, 291.
(25) (a) Islam, M. S. *J. Mater. Chem.* **2000**, *10*, 1027.(b) Islam, M. S.; Slater P. R. MRS Bull. **2009**, in press.
(26) (a) Kendrick, E.; Kendrick, J.; Knight, K. S.; Islam, M. S.; Slater, P. R. *Nat. Mater.* **2007**, *6*, 871. (b) Tolchard, J. R.; Slater, P. R.; Islam, M. S. *Adv. Funct. Mater.* **2007**, *17*, 2564.

parameters from Dominko et al.;[8] this structure has unusually short Li−Si distances of 2.5 Å as pointed out by Politaev et al.[12] Interestingly, from analysis of our calculated relaxed structure these Li−Si distances have lengthened to a more realistic 3.0 Å and are close to the observed values for Li_2FeSiO_4 from Nishimura et al.[7]

In general, the good reproduction of the complex structures of both monoclinic and orthorhombic polymorphs of Li_2MnSiO_4 provides us with confidence that the potential model can be used reliably in the defect and diffusion simulations.

3.2. Intrinsic Defects. As noted, a greater insight into the defect properties of electrode materials is crucial to the full understanding of their electrochemical behavior. A series of isolated point defects (vacancy and interstitial) energies were calculated, which were combined to determine the formation energies for Frenkel and Schottky-type defects in Li_2MnSiO_4. The following equations represent the reactions involving these defects as written using Kröger-Vink notation.

Li Frenkel: $$Li_{Li}^{\times} \rightarrow V_{Li}' + Li_i^{\bullet} \quad (3)$$

Mn Frenkel: $$Mn_{Mn}^{\times} \rightarrow V_{Mn}'' + Mn_i^{\bullet\bullet} \quad (4)$$

O Frenkel: $$O_o^{\times} \rightarrow V_o^{\bullet\bullet} + O_i'' \quad (5)$$

Schottky: $$2Li_{Li}^{\times} + Mn_{Mn}^{\times} + Si_{Si}^{\times} + 4O_o^{\times} \rightarrow 2V_{Li}' + V_{Mn}'' + V_{si}'''' + 4V_o^{\bullet\bullet} + Li_2MnSiO_4 \quad (6)$$

We also examined the Li/Mn "anti-site" pair defect involving the interchange of an Li^+ (radius 0.74 Å) with an Mn^{2+} ion (radius 0.83 Å), which is worth investigating since "cation exchange" effects have been a topic of discussion.[5,12] This process can be described by the following equation:

$$Li_{Li}^{\times} + Mn_{Mn}^{\times} \rightarrow Li_{Mn}' + Mn_{Li}^{\bullet} \quad (7)$$

Off-stoichiometry defects (lithium deficiency or oxygen excess) were also considered according to the following intrinsic oxidation reactions:

$$2Li_{Li}^{\times} + \frac{1}{2}O_2 \rightarrow 2V_{Li}' + 2h^{\bullet} + Li_2O \quad (8)$$

$$\frac{1}{2}O_2 \rightarrow O_i'' + 2h^{\bullet} \quad (9)$$

Our approach to electronic defects follows that used for other transition metal compounds (e.g., $LiMPO_4$ where M = Mn, Fe, Co, Ni)[18,19] in which we model the localized hole ($h^{\bullet}$) species (small polaron) on manganese as Mn^{3+}. We recognize that there will be Mn(3d)−O(2p) mixing, but our main concern here is to assess the relative reaction energetics that create hole species, for which these methods have proved valuable. All the energies for these intrinsic defect processes (eqs 3−9) were derived by combining the calculated energies of isolated point defects and lattice energies and are listed in Table 3.

Table 2. Calculated and Experimental Structural Parameters and Mean Bond Distances for Monoclinic and Orthorhombic Li_2MnSiO_4

(a) Monoclinic ($P2_1/n$)[a]

parameter	calc	expt
a (Å)	6.4211	6.3361
b (Å)	10.9941	10.9146
c (Å)	5.047	5.0730
β (deg)	90.982	90.987
Li1−O (Å)	2.012	1.974
Li2−O (Å)	2.049	2.042
Mn−O (Å)	2.047	2.040
Si−O (Å)	1.633	1.654

(b) Orthorhombic ($Pmn2_1$)[b]

parameter	calc	initial
a (Å)	6.4237	6.3109
b (Å)	5.3474	5.3800
c (Å)	4.9369	4.9662
Li−O (Å)	1.982	1.982
Mn−O (Å)	2.075	1.970
Si−O (Å)	1.635	1.737

[a] ref 12. [b] refs 5, 8 based on Li_2FeSiO_4

Table 3. Energies of Intrinsic Defects in Li_2MnSiO_4

		energy (eV)	
defect	equation	monoclinic	orthorhombic
Li Frenkel	3	2.55	3.90
Mn Frenkel	4	6.41	7.79
O Frenkel	5	8.11	11.78
Full Schottky	6	34.84	43.73
Li/Mn anti-site	7	1.38	1.65
Li^+ deficiency (oxidation)	8	14.36	16.12
oxygen excess (oxidation)	9	12.43	14.75

Three main points emerge from the results. First, the most favorable intrinsic disorder for both structures is the Li−Mn anti-site defect (eq 7); no significant changes in the local cation-oxygen bond lengths are found around these defects. These results suggest that there will be a small percentage of Li on Mn sites (Li_{Mn}') and Mn on Li sites ($Mn_{Li}^{\bullet}$); the exact concentration would be temperature dependent and hence sensitive to synthesis routes, processing conditions, and thermal history. Interestingly, Politaev et al.[12] have observed a small but nonzero amount of Mn substituting for Li and vice versa in monoclinic Li_2MnSiO_4. From electrochemical studies on the related Li_2FeSiO_4 system, Nyten et al.[5] observe a shift in the potential plateau between first and second cycles, and they suggest that this is related to structural rearrangement involving interchange of some of the Li and Fe ions.

Second, the formation of Mn Frenkel, O Frenkel, and Schottky defects is unfavorable in both structures. In particular, oxygen vacancies and oxygen interstitials are highly unfavorable and thus unlikely to occur in any significant concentration in the pure material.

Finally, the high energies for the intrinsic oxidation processes suggest that the formation of hole species and oxygen interstitials is difficult. This agrees with the observation that this material does not show significant

oxygen nonstoichiometry and is consistent with the structural stability of the SiO_4 polyanion matrix.

3.3. Lithium Ion Mobility. The intrinsic lithium ion mobility in and out of the Li_2MnSiO_4 material is of crucial importance when assessing its use as a possible high-rate cathode material in lithium batteries. However, the diffusion paths in the Li_2MnSiO_4 polymorphs have not been clearly established. Using atomistic simulation techniques it is possible to examine various possible diffusion paths responsible for lithium ion conduction, which are often difficult to probe on the atomic scale by experiment alone.

For the monoclinic structure, we have identified four main migration paths between adjacent Li sites (illustrated in Figure 2): path A is between Li1 and Li2 sites with the shortest jump distance of about 2.7 Å; path B is in the *ab* plane with a jump distance of about 2.9 Å; paths C and D are also between Li1 and Li2 sites, but with longer jump distances of 3.5 Å. For the orthorhombic structure, we have identified two main migration paths (illustrated in Figure 3): path X is parallel to the *c* axis with a zigzag trajectory, and path Y is parallel to the *a* axis. We should add that we have considered a range of other paths with longer Li−Li migration distances of >4 Å, but these were all found to have prohibitively high migration barriers (>2.5 eV).

Energy profiles for these mechanisms can be derived by calculating the energy of the migrating ion along the diffusion path. Relaxation of the surrounding lattice (>700 ions) as an ion migrates through the structure is treated explicitly by these defect modeling methods. The position of highest potential energy along the migration path corresponds to the activation energy of migration, E_{mig}. The calculated migration energies and the Li−Li jump distances for the two structures are listed in Table 4.

There are two key points from the results. First, the lowest migration energies are 0.54 eV (path B) and 0.60 eV (path A) for the monoclinic structure and 0.95 eV (path X) for the orthorhombic structure. This suggests a higher Li mobility in the monoclinic structure. Such differences in Li mobility would influence the ability to extract lithium from the two polymorphs and hence lead to differences in rate capability and general electrochemical behavior. An important related feature is the observed structural rearrangement upon cycling and the possible coexistence of the two structural polymorphs in the as-prepared Li_2MnSiO_4.[12] Although there are no Li-ion conductivity data for this system for direct comparison, our calculated value of about 0.5−0.6 eV for the monoclinic polymorph is consistent with experimental activation energies in other framework-structured or LISICON-type materials.[27]

Second, these results indicate the anisotropic nature of Li ion conduction in this material, which is probably general for the Li_2MSiO_4 (M = Mn, Fe, Co) family of compounds.

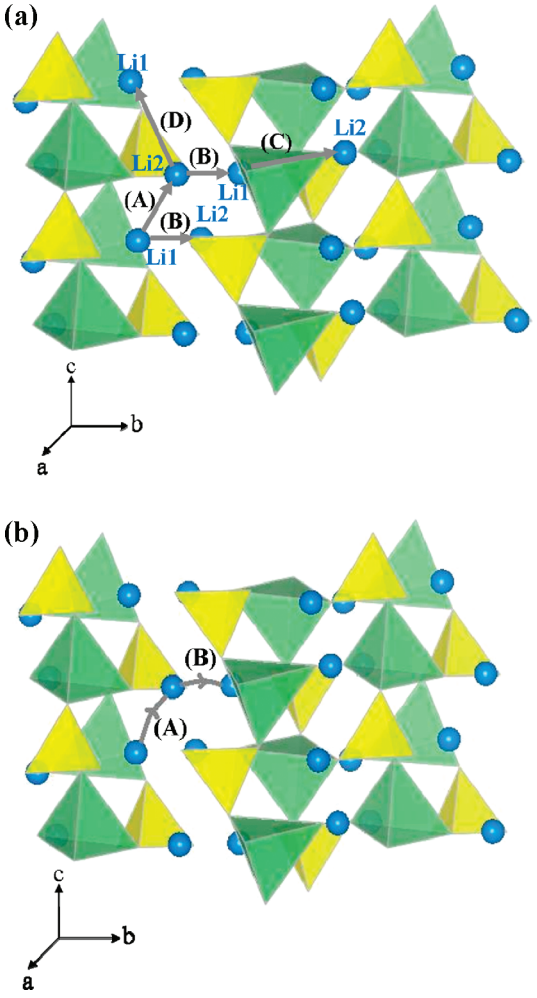

Figure 2. Lithium ion migration in monoclinic Li_2MnSiO_4; (a) migration paths and (b) schematic of lowest energy paths (A and B) showing the curved trajectory between Li sites.

It is also often assumed that the migrating ion takes the shortest linear path between adjacent Li sites. However, detailed analysis of our simulations for the favored migration mechanisms (A, B, and X) reveals a small deviation from the linear (straight) route involving a curved path between adjacent sites (shown in Figures 2 and 3). In each case, the migrating ion deviates from a linear path by around 0.3 Å at its midpoint, while there is also a small amount of lattice relaxation around the diffusing lithium ion as it passes close to SiO_4 and MnO_4 tetrahedra.

Although it is very difficult to obtain corresponding experimental information, we note that recent studies of the related $LiFePO_4$ cathode material[28] combining neutron diffraction and the maximum entropy method show a curved Li migration pathway, in agreement with our earlier simulation results on the phosphate.[18]

Our defect calculations suggest that Li/Mn anti-site defects are intrinsic to Li_2MnSiO_4, and there is experimental evidence of a low concentration of Li/Mn cation exchange in Li_2MnSiO_4.[12] Therefore, such cation mixing with Li on Mn sites and Mn on Li sites may either

(27) (a) Sebastion, L.; Gopalakrishnan, J. *J. Mater. Chem.* **2003**, *13*, 433. (b) Thangadurai, V; Kaack, H; Weppner, W. J. F. *J. Am. Ceram. Soc.* **2003**, *86*, 437.

(28) Nishimura, S.; Kobayashi, G.; Ohayama, K.; Kanno, R.; Yashima, M.; Yamada, A. *Nat. Mater.* **2008**, *7*, 707.

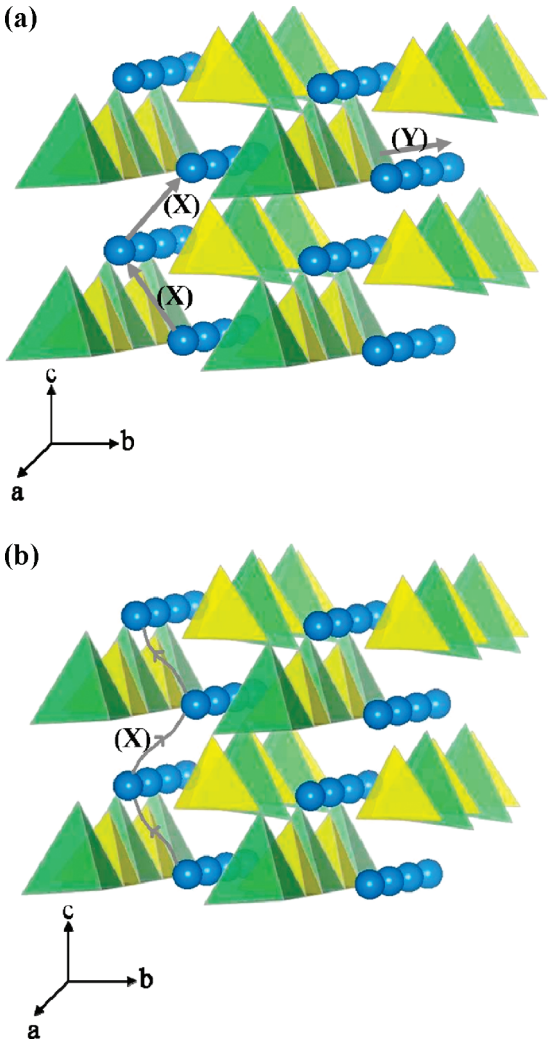

Figure 3. Lithium ion migration in orthorhombic Li_2MnSiO_4; (a) migration paths and (b) schematic of lowest energy path (X) showing the curved trajectory between Li sites.

Table 4. Pathways and Energies of Lithium-Ion Migration in Li_2MnSiO_4

path	Li−Li separation (Å)	E_{mig} (eV)
	(a) Monoclinic	
Li1−Li2 (A)	2.69	0.60
Li2−Li1 (B)	2.90	0.54
Li1−Li2 (C)	3.50	1.58
Li1−Li2 (D)	3.53	0.94
	(b) Orthorhombic	
Li−Li (X)	3.10	0.95
Li−Li (Y)	3.22	1.29

facilitate or block diffusion pathways. Either scenario would likely affect the rate capability and capacity retention of the electrode material.

We have therefore carried out preliminary simulations on anti-site cation migration of both Li'_{Mn} and $Mn^{\bullet}_{Li}$ to adjacent vacant Li sites. This process can be viewed as an exchange of an anti-site cation with a neighboring lithium vacancy; the lithium vacancy would then continue to migrate in the opposite direction. Very similar simulations were reported in previous work on anti-site migration in the olivine-type materials $LiMPO_4$ (M = Mn, Fe, Co, Ni).[19]

Table 5. Energies for Anti-Site Cation ($Li'_{Mn}$and $Mn^{\bullet}_{Li}$) Migration in Li_2MnSiO_4

	E_{mig} (eV)	
anti-site cation	monoclinic	orthorhombic
$Li'_{Mn} \rightarrow V'_{Li}$	0.80	0.48
$Mn^{\bullet}_{Li} \rightarrow V'_{Li}$	1.16	1.93

The lowest barrier energies listed in Table 5 suggest favorable Li'_{Mn} anti-site migration, particularly for the orthorhombic structure. These defects could therefore facilitate long-range diffusion if there was a significant population of Li on Mn sites. In contrast, however, migration energies of the $Mn^{\bullet}_{Li}$ anti-site cation are greater than 1.1 eV, suggesting that Mn on Li sites would impede Li diffusion.

We recognize there is still debate concerning the observed structures of the Li_2MnSiO_4 material as-prepared and upon cycling, which would affect any Li/Mn mixing or structural rearrangement; this warrants further experimental investigation. Future atomistic modeling work will include examining further the effect of Li/Mn partial exchange and the use of DFT and molecular dynamics (MD) techniques.

3.4. Trivalent Dopant Substitution. A possible approach to increasing the amount of lithium extracted (and hence to enhance the capacity) of the Li_2MnSiO_4 cathodes is to incorporate extra lithium into the as-prepared materials, although very little work has been performed in this area. In this study, we have examined trivalent doping (Al and Ga) on the Si site to assess the energetics of dopant incorporation with extra lithium for charge compensation.

Our simulation methods can probe these issues by generating quantitative data on the relative energies of different modes of dopant substitution. This can provide a useful systematic guide to the site-selectivity for different dopant species and to trends in dopant solubility.

For Al^{3+} and Ga^{3+} doping on the Si site, charge compensation was achieved through creating Li interstitials, which was found to be more favorable than hole compensation by over 3 eV. Our initial calculations find that the lowest energy compensation mechanism for trivalent dopant substitution at Li or Mn sites is Mn vacancies; these three processes can be described by the following defect equations using Al^{3+} as the example dopant ion:

Si site:
$$\frac{1}{2}Al_2O_3 + Si^{\times}_{Si} + \frac{1}{2}Li_2O \rightarrow Al_{Si}' + Li_i^{\bullet} + SiO_2 \quad (10)$$

Mn site:
$$\frac{1}{2}Al_2O_3 + \frac{3}{2}Mn^{\times}_{Mn} \rightarrow Al^{\bullet}_{Mn} + \frac{1}{2}V''_{Mn} + \frac{3}{2}MnO \quad (11)$$

Li site:
$$\frac{1}{2}Al_2O_3 + Li^{\times}_{Li} + Mn^{\times}_{Mn} \rightarrow Al^{\bullet\bullet}_{Li} + V''_{Mn} + \frac{1}{2}Li_2O + MnO \quad (12)$$

The energies of these dopant substitution reactions were calculated by combining the appropriate defect and lattice energy terms. Interatomic potentials used to model the corresponding binary oxides of the dopant cations were used in each case (listed in Table 6). The dopant calculations were also carried out at the dilute limit, as is appropriate for examining low dopant concentrations. These potentials and this systematic

Table 6. Interatomic Potential Parameters (Rigid Ion) for Al and Ga Dopants

interaction	A (eV)	ρ (Å)	C (eV·Å^6)	oxide lattice energy (eV)
$Al^{3+}\cdots O^{2-}$	1114.9	0.3118	0	−161.00
$Ga^{3+}\cdots O^{2-}$	2901.12	0.2742	0	−156.60

Table 7. Calculated Energies of Trivalent Dopant Incorporation in Li_2MnSiO_4

	energy (eV)					
	Li site		Mn site		Si site	
dopant	mono[a]	ortho[b]	mono[a]	ortho[b]	mono[a]	ortho[b]
Al^{3+}	9.60	9.13	4.95	5.15	2.70	3.51
Ga^{3+}	11.79	9.16	5.09	5.10	3.90	4.74

[a] Mono = monoclinic ($P2_1/n$). [b] Ortho = orthorhombic ($Pmn2_1$).

approach to dopant incorporation have been applied successfully to other oxide and silicate systems.[19,26]

The energies for Al^{3+} and Ga^{3+} doping at all three cation sites are presented in Table 7. The results indicate that the most favorable dopant incorporation energy is found for Al^{3+} on the Si site in the monoclinic structure with Li interstitial compensation (eq 10). This suggests a possible synthesis-doping strategy of introducing additional lithium into Li_2MnSiO_4, although the exact amount of Al incorporation cannot be predicted. Of course, the ideal scenario would be $x = 1.0$ for the solid solution $Li_{2+x}MnSi_{1-x}Al_xO_4$, which could permit the removal of two Li^+ from the structure accompanied by oxidation of Mn^{2+} to Mn^{4+}, giving a high capacity to store charge (ca. 300 mA h g^{-1}); this could possibly lead to a lithium battery with an energy density higher than those using $LiMn_2O_4$ or $LiFePO_4$, while leaving one lithium behind for structural integrity.

The magnitude of the energies for Ga versus Al on the Si site suggests a relatively low degree of Ga dopant solubility. Perhaps not surprisingly, the results indicate that both Al and Ga substitution on the Li site is highly unfavorable for both structures.

4. Conclusions

This systematic survey of both monoclinic and orthorhombic structures of Li_2MnSiO_4 has used atomistic simulation techniques to provide detailed insights into intrinsic defects, lithium ion mobility, and trivalent doping, which are relevant to the general electrochemical behavior of orthosilicates as lithium battery cathodes. The main results can be summarized as follows:

(1) Our simulations show good reproduction of the observed monoclinic ($P2_1/n$) and orthorhombic ($Pmn2_1$) structures of Li_2MnSiO_4. Interestingly, for our calculated optimized structure of the orthorhombic polymorph, the initial short Li−Si distances of 2.5 Å have lengthened to 3.0 Å.

(2) The most favorable intrinsic disorder type for both structures is the Li−Mn anti-site defect. This suggests that there will be a population of Li on Mn sites (Li'_{Mn}) and Mn on Li sites ($Mn^{\bullet}_{Li}$); the exact concentration would be temperature dependent and hence sensitive to synthesis routes and thermal history. These results are also significant in relation to the electrochemically driven structural rearrangement upon cycling involving some Li/Mn site interchange, which needs further experimental characterization. The high energies for the intrinsic oxidation processes suggest that the formation of hole species and oxygen interstitials is difficult. This accords with the observation that Li_2MnSiO_4 does not show significant oxygen nonstoichiometry.

(3) The lowest activation energies for Li migration in the monoclinic and orthorhombic structures are 0.54 and 0.95 eV, respectively. Such differences in intrinsic Li mobility would influence the ability to extract lithium from the two polymorphs and hence lead to contrasting rate capability and capacity retention as rechargeable electrodes. A related feature is the possible coexistence of the two structural polymorphs or the presence of structural intergrowths in the as-prepared Li_2MnSiO_4. Our results show curved conduction paths and anisotropic Li transport, which are probably general for the Li_2MSiO_4 (M = Mn, Fe, Co) orthosilicate family of compounds.

(4) Li/Mn anti-site defects or cation exchange will influence Li transport. Preliminary results indicate relatively favorable Li'_{Mn} anti-site migration energies, which could facilitate long-range diffusion especially in the orthorhombic structure. In contrast, migration barriers for the $Mn^{\bullet}_{Li}$ anti-site cation are greater than 1.1 eV, suggesting that Mn on Li sites would impede Li conduction.

(5) The most favorable dopant incorporation is found for Al^{3+} on the Si site in the monoclinic structure with Li interstitial compensation. This suggests a possible synthesis-doping strategy for introducing extra lithium to form the $Li_{2+x}MnSi_{1-x}Al_xO_4$ system; this could permit the removal of more Li^+ from the structure and hence increase the capacity, and warrants further investigation. Indeed, one of the aims of this study is to stimulate complementary experimental work on this important new family of lithium battery materials.

Acknowledgment. We thank the EPSRC for funding as part of the SUPERGEN Energy Storage Consortium (grant code EP/D031672/1) and the Materials Chemistry Consortium for HECToR supercomputer facilities. We also acknowledge Rob Armstrong (St. Andrews, UK), Josh Thomas (Uppsala, Sweden) and Anti Liivat (Uppsala, Sweden) for useful discussions.

Note Added after ASAP Publication. Due to a production error, this paper published ASAP on October 9, 2009 with an error in the title; the corrected version published ASAP October 12, 2009.